PHYSICAL REVIEW B VOLUME 35, NUMBER 5 15 FEBRUARY 1987-I

Resonant Raman study of intrinsic defect modes in electron- and neutron-irradiated GaAs

R. S. Berg
Department of Physics, Wellesley College, Wellesley, Massachusetts 02181

P. Y. Yu
Department of Physics, University of California, Berkeley, California 94720
and Center for Advanced Materials, Lawrence Berkeley Laboratory, University of California, Berkeley, California 94720
(Received 17 July 1986)

We report the results of a resonant Raman study of GaAs samples which contain $\sim 10^{17}$–10^{18} cm^{-3} intrinsic defects that have been introduced by either electron or neutron irradiation. We observe several defect-related modes, two of which we identify as local modes of an intrinsic defect, most likely an As vacancy. In the vicinity of the E_0 transition we observe enhancements of these modes that are more dispersive than the enhancement of the TO-phonon scattering. We explain these observations phenomenologically with a fourth-order perturbation theory involving elastic scattering of either an electron or a hole by a defect. The theory predicts that strongly dispersive enhancement can occur for vibrational modes that involve enhanced motion of atoms in the immediate vicinity of a defect.

I. INTRODUCTION

There is currently much interest in the microscopic identity of intrinsic defects in GaAs.[1] Raman scattering has the potential to provide microscopic information regarding the properties of these defects.[2] For example, lattice vibrations are sensitive to local environments, and so it is possible to use Raman scattering to obtain structural information about a point defect.[3]

In spite of this potential, the use of Raman scattering has been limited by its relatively low sensitivity due to the small scattering cross sections. This limitation is particularly severe for the case of defects in semiconductors since the defect concentrations in situations of interest are usually very low (<1 ppm). In this paper we overcome this drawback by tuning the incident photon energies to just below the fundamental band gap. We are thus able to take advantage of the relatively large scattering volume and strong resonant enhancement in the Raman cross section. The latter phenomenon is known as resonant Raman scattering (RRS). In addition to increasing the size of the signal, the enhancement profile of the Raman modes also provides valuable information on the nature of the defects and on their Raman scattering mechanisms.

Several previous studies have focused on the RRS behavior of defect-related modes in semiconductors. Bedel *et al.*[4] studied the resonance behavior of defect-induced first-order Raman scattering in the alloy system $InAs_xP_{1-x}$ in the vicinity of the E_1 transition. They observed a relatively small resonant enhancement for these modes. Yu *et al.*[5] studied RRS CdS:Cl. They tuned the energy of the scattered photons through an exciton bound to a shallow acceptor. By observing a large enhancement in the Raman scattering of a V_{Cd}-Cl_S complex they were able to deduce that such complexes form shallow acceptors in CdS. Wolford *et al.*[6] used this technique to study the deep level N in $Al_xGa_{1-x}As$. Usually in these III-V alloys inhomogeneous broadening due to differences in the local environment prevents much useful information from being obtained from the defect-assisted recombination luminescence. However, by tuning the incident photon energy, Wolford *et al.* were able to circumvent the inhomogeneous broadening by selectively exciting only a narrow distribution of the N centers. By examining the details of the now observable phonon replicas, they were able to deduce information concerning the electronic wave function of the N level.

In this paper we report the results of a resonant Raman study of GaAs samples which contain intrinsic defects that have been introduced by either electron or neutron irradiation. We observe several defect-related modes, two of which we identify as local modes of an intrinsic defect. In the vicinity of the fundamental absorption edge (E_0 transition) we observe enhancements of these modes that are more strongly dispersive than the enhancement of the TO-phonon scattering. The experimental results have been explained phenomenologically with a fourth-order perturbation theory involving elastic scattering of either an electron or a hole by a defect.

This paper is organized as follows. In Secs. II and III we review the microscopic theories of RRS in a perfect crystal and in the presence of defects, respectively. In Sec. IV we describe our experimental technique, Sec. V contains our experimental results, Sec. VI discusses these results, and Sec. VII presents our conclusions.

II. MICROSCOPIC THEORY OF RESONANT RAMAN SCATTERING IN A PERFECT CRYSTAL

A. General description

Before presenting the microscopic theories of defect-induced scattering, it is first necessary to review the mi-

croscopic theory of RRS in a perfect crystal. First-order Raman scattering involves a third-order perturbation process with two virtual intermediate states $|a\rangle$ and $|b\rangle$. For semiconductors and insulators, $|a\rangle$ is a state in which an electron is excited from the valence band to the conduction band via the absorption of an incident photon ω_i. $|b\rangle$ is a state which results when the excited electron or hole in $|a\rangle$ is scattered into another state by a phonon. When the electron and hole in $|b\rangle$ recombine, the scattered photon ω_s is emitted. This process can be represented by a Feynman diagram of the type shown in Fig. 1(a). The transitions involved can occur in any time order, giving rise to six terms in the scattering cross section. Under resonant conditions it can be shown that the diagram in Fig. 1(a) is the most important one so the total cross section for scattering a photon into a solid angle $d\Omega$ via emission or absorption of a phonon of frequency ω_p can be written as

$$\sigma=\frac{2\pi}{\hbar^6}D(\omega_p)\sum_{k_s}\left|\sum_{a,b}\frac{\langle f|H_{\rm ER}|b\rangle\langle b|H_{\rm EP}|a\rangle\langle a|H_{\rm ER}|i\rangle}{(\hbar\omega_a-\hbar\omega_i)(\hbar\omega_b-\hbar\omega_s)}\right|^2\delta(\omega_i\mp\omega_p-\omega_s)\,, \tag{1}$$

where $H_{\rm ER}$ and $H_{\rm EP}$ are the interaction Hamiltonians between the electron and the photon and the electron and the phonon, respectively; the $(+)$ and $(-)$ signs correspond to absorption (anti-Stokes Raman process) and emission (Stokes Raman process) of a phonon, respectively; $D(\omega_p)$ is the phonon density of states; and $\hbar\omega_a$ and $\hbar\omega_b$ are the energies of the intermediate states $|a\rangle$ and $|b\rangle$, respectively. For the diagram shown in Fig. 1(a), $\hbar\omega_a=\hbar\omega_0+\hbar\omega_1+\hbar\omega_3$ and $\hbar\omega_b=\hbar\omega_0+\hbar\omega_2+\hbar\omega_3$, where $\hbar\omega_0$ is the band-gap energy, $\hbar\omega_j$ $(j=1,2)$ denotes the ener-

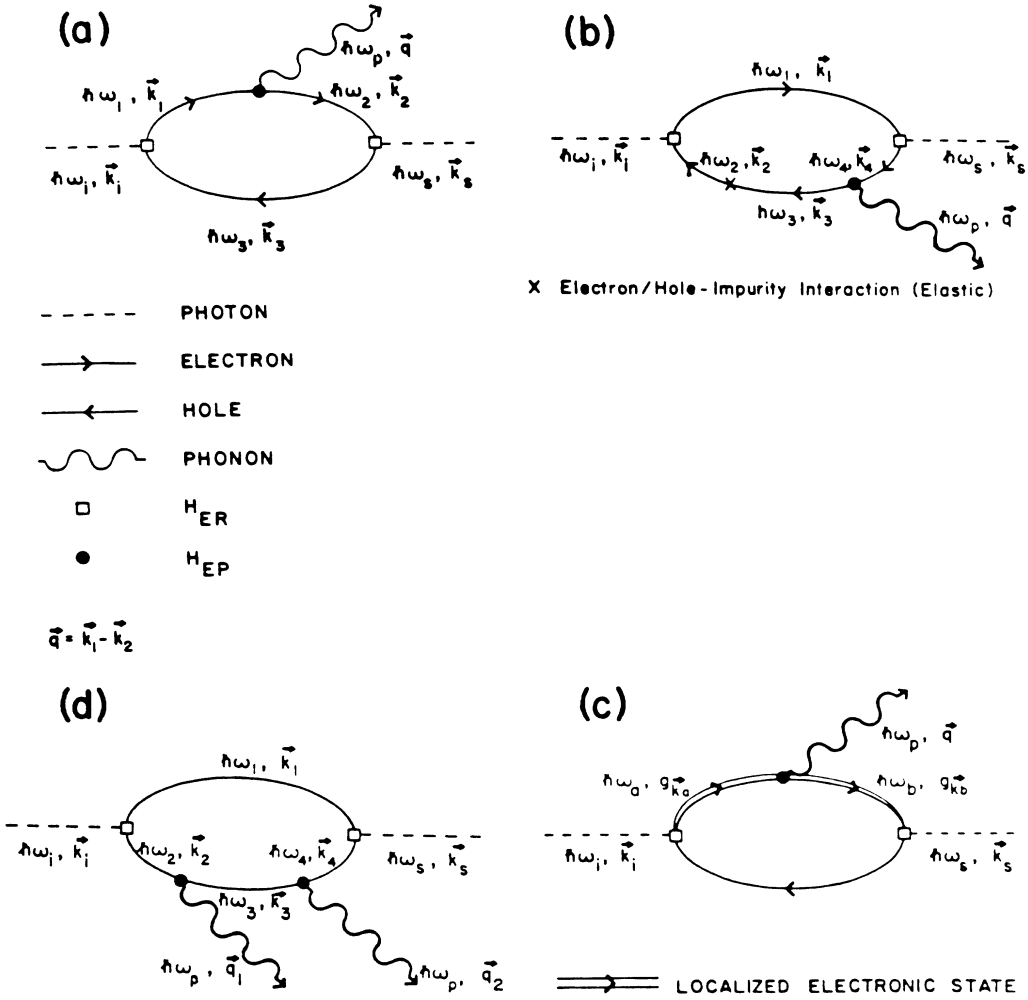

FIG. 1. Feynman diagrams for various Raman processes discussed in the text. (a) Third-order Raman process in a crystalline semiconductor; (b) fourth-order defect-mediated process; (c) KTE mechanism involving localized intermediate electronic states; (d) fourth-order two-phonon scattering process considered by Zeyher (see Ref. 18).

gy of the electron, and $\hbar\omega_3$ is the energy of the hole relative to their respective band extrema. In a perfect crystal quasimomentum is conserved at each vertex of the diagram in Fig. 1(a). Therefore $\mathbf{k}_i - \mathbf{k}_s = \mathbf{q}$, where $\mathbf{k}_i$, $\mathbf{k}_s$, and $\mathbf{q}$ are the wave vectors of the incident photon, the scattered photon, and the emitted $(+)$ or absorbed $(-)$ phonon, respectively. The summation over $\mathbf{k}_s$ in Eq. (1) includes only those photons scattered into the solid angle $d\Omega$.

When the incident photon energy coincides with the energy of an electronic transition, the energy denominator in Eq. (1) becomes very small (an imaginary damping component added to the electronic energies prevents the cross section from becoming infinite) so the cross section becomes very large. This is the explanation for the enhancement in the cross section that occurs under resonant conditions. Let us first consider a special case of Eq. (1) where there is a single isolated intermediate state whose energy and damping are $\hbar\omega_0$ and $\hbar\Gamma$ respectively. In this case Eq. (1) reduces to

$$\sigma(\omega_i) \propto \left| \frac{i\Gamma}{(\omega_0-\omega_i+i\Gamma)(\omega_0-\omega_s+i\Gamma)} \right|^2 . \quad (2)$$

The behavior of the cross section as a function of incident photon frequency in the vicinity of ω_0 is depicted on the right-hand side of Fig. 2(a). The two identical peaks located at ω_0 and $\omega_0+\omega_p$ (solid line) are referred to as the ingoing and outgoing resonances, respectively. In this case only one of the two factors in the denominator of Eq. (2) vanishes at a time. When $\Gamma \gtrsim \omega_s - \omega_i$, the two peaks broaden and merge into one peak which is symmetric about $\omega_0+\omega_p/2$ (dashed line).

In general, above the band gap of a semiconductor there is a continuum of intermediate states and it is necessary to sum over these states in Eq. (1). The behavior of the ingoing and outgoing resonances in this case is shown in Fig. 2(b). $\sigma(\omega_i)$ again exhibits peaks at $\omega_i=\omega_0$ and $\omega_i=\omega_0+\omega_p$. In contrast to the example in Fig. 2(a), these two peaks are no longer identical. This is because when $\omega_s=\omega_0$ (the outgoing resonance), there is the possibility that the incident photon can also excite a real transition. Thus both terms in the denominator of Eq. (1) can simultaneously be very small (double resonance). Such a double resonance is clearly not possible at the ingoing resonance. The result is that the outgoing resonance can be much stronger than the ingoing resonance. Therefore even when damping merges the two peaks at ω_0 and $\omega_0+\omega_p$ into a single peak, this peak still tends to occur at the outgoing resonance due to the effect of double resonance.

Double-resonance effects are strongest when it is possible to conserve energy in all of the steps in the Raman process. This is the situation that is depicted in Fig. 2(b) for the outgoing resonance. Ordinarily in a one-phonon Raman process the phonon momentum is small so the restrictions imposed by momentum conservation prevent this from occurring. This is the situation shown in Fig. 2(c).

Next we consider two specific cases of RRS in a perfect crystal, viz. allowed TO-phonon scattering and forbidden LO-phonon scattering.

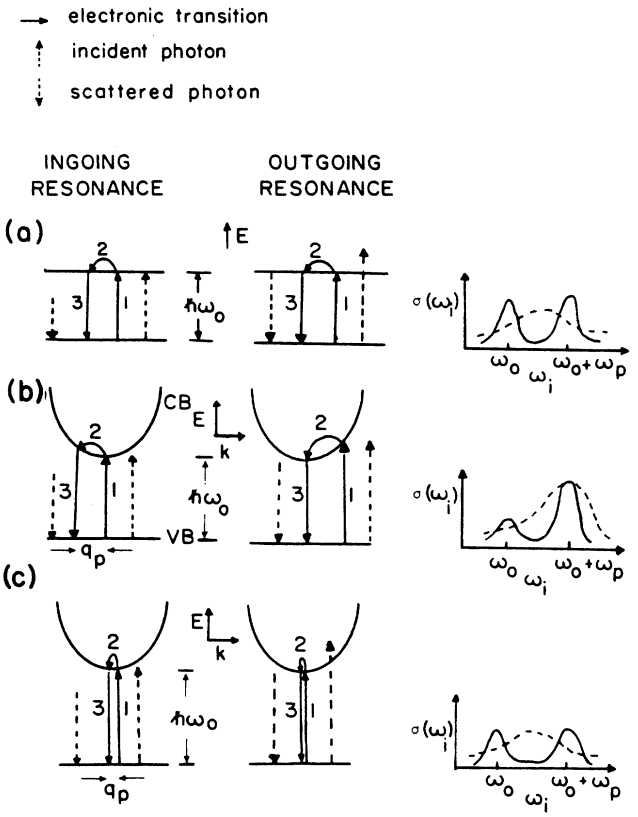

FIG. 2. Demonstration of ingoing (first column) and outgoing (second column) resonances and the occurrence of double resonance. These drawings depict several possible cases of resonance associated with the Feynman diagram in Fig. 1(a). The numbers indicate the time order of the electronic transitions. It is assumed that step 2 involves the emission of a phonon of energy $\hbar\omega_p$ and wave vector $\mathbf{q}_p$ by the electron. The length of the photon arrows denote the photon energy. The third column shows the expected behavior of $\sigma(\omega_i)$ for small damping (solid lines) and larger damping (dashed line). (a) One discrete intermediate state, (b) a two-band model that allows double resonance to occur at the outgoing resonant, (c) a two-band model where double resonance is not possible.

B. Allowed TO-phonon scattering

Calculations of the resonance behavior of this type of scattering in the vicinity of a three-dimensional critical point (such as the E_0 transition) in zincblende-type semiconductors have been performed by a number of authors.[7-9] Here we summarize the results presented by Cardona.[8] We take as our starting point Eq. (2), which includes only the most resonant term. Cardona's treatment includes some less dispersive terms which do not appreciably affect the line shape close to resonance. The following assumptions were made in obtaining these results.

(1) Only two-band terms are included. In GaAs the $E_0+\Delta_0$ transition, which lies closest to the E_0 transition, is 2400 cm^{-1} higher in energy. Since this separation is large compared to $\omega_{TO}=270$ cm^{-1}, the three-band terms

can be neglected.

(2) The matrix elements in Eq. (1) are assumed to be independent of ω_a and can therefore be taken outside of the summation.

(3) The conduction and valence bands of GaAs are assumed to be parabolic and their dispersions are given by

$$\omega_{c(v)}=\frac{\hbar k^2}{2m_{c(v)}}\ , \tag{3}$$

where $m_{c(v)}$ is the effective mass of the conduction (valence) band. For the valence band an appropriately averaged mass m_v is used for the heavy-hole band.

(4) The electronic states have zero damping.

With these approximations Cardona's result reduces to

$$\sigma_{\mathrm{TO}}(\omega_i)\propto\frac{1}{\Delta^2}\left|\frac{F\left[\frac{x}{1+\Delta}\right]}{(1+\Delta)^{3/2}}-\frac{F\left[\frac{x}{1-\Delta}\right]}{(1-\Delta)^{3/2}}\right|^2\ , \tag{4}$$

where

$$\Delta\equiv\omega_p/2\omega_0,\quad x\equiv\frac{\omega_i}{\omega_0+\omega_p/2},\ \text{and}\ F(x)\equiv\frac{(1-x)^{1/2}}{x^2}\ .$$

A plot of this result with parameters appropriate for the TO phonon and band gap of GaAs is shown in Fig. 3. The two structures occurring at $\omega_i=\omega_0$ and $\omega_s=\omega_0$ correspond to the ingoing and outgoing resonances. The line shape is approximately symmetrical. This is because the double-resonance effect is not significant in this case due to the constraints imposed by quasimomentum conservation [c.f. Fig. 2(c)].

The effect of damping can be incorporated by adding an imaginary part Γ to the frequency ω_0. The resulting effect is significant only when Γ is appreciable compared to ω_p. Otherwise, the width of the resonance is roughly ω_p.

C. Forbidden LO-phonon scattering

The appearance of LO-phonon scattering in geometries where they are forbidden according to the standard selection rules is well documented.[8] Such forbidden scattering has been found to exhibit very strong resonant enhancements near transitions such as E_0 and $E_0+\Delta_0$. Away from resonance the forbidden scattering becomes negligible. Also it has been observed experimentally that the forbidden scattering exhibits predominantly Γ_1 symmetry, i.e., the scattered light is polarized parallel to the incident light. Many authors have attempted to explain the forbidden scattering in perfect crystals. Again we summarize here the results presented by Cardona.[8]

The underlying reason for the forbidden LO scattering is the macroscopic electric field E associated with an LO phonon. The interaction energy of an electron (hole) in the presence of this field was shown by Fröhlich to be $-(+)ieE/q$, where $\hbar q$ is the phonon quasimomentum. It is the q dependence of the interaction that accounts for the forbidden scattering. By substituting this q-dependent Fröhlich matrix element into Eq. (1), one can show that

$$\sigma_{\mathrm{LO}}(\omega_i)\propto\left|\frac{1}{|\mathbf{q}|}\left[\Xi(qS_c)-\Xi(qS_v)\right]\right|^2\ , \tag{5}$$

where

$$\Xi(\mathbf{q})=(4\pi|\mathbf{q}|)^{-1}\tan^{-1}\{i\mathbf{q}(2m^*)^{-1/2}\omega_{\mathrm{LO}}{}^{-1}[(\omega_i-\omega_0)^{1/2}-(\omega_s-\omega_0)^{1/2}]\}\ ,$$

$$S_{c(v)}=\frac{m_{c(v)}}{m_c+m_v},\quad (m^*)^{-1}=m_c{}^{-1}+m_v{}^{-1}\ .$$

For small q the intensity of the scattering is found to be quadratic in q. Shown in Fig. 3 is the behavior of $\sigma_{\mathrm{LO}}(\omega_i)$ predicted by Eq. (5) using parameters appropriate to the E_0 transition in GaAs. The line shape is again symmetrical about $\omega_0+\omega_{\mathrm{LO}}/2$, indicating that double-resonance effects are not strong in this case either. Note that the forbidden LO-phonon cross section falls rapidly to zero on either side of the resonance peak while the allowed TO-phonon cross section decreases much more slowly.

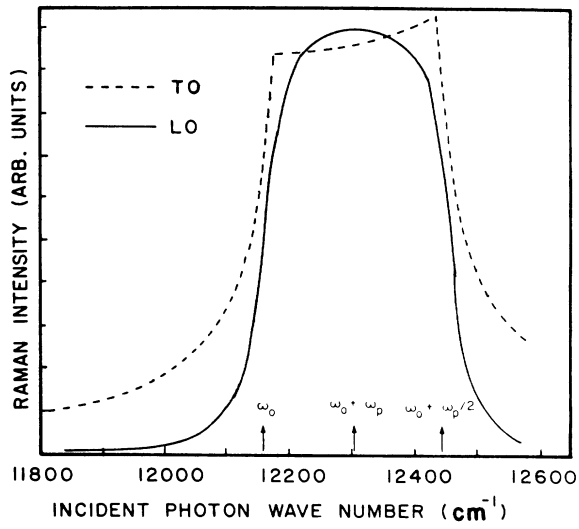

FIG. 3. Theoretically predicted scattering intensity for the TO phonon [from Eq. (4)] and for the forbidden LO-phonon scattering [Eq. (5)] in GaAs at the E_0 energy gap. Both curves are in the limit of zero damping.

In addition to the above intrinsic mechanism involving the q-dependent Fröhlich interaction, a number of authors has proposed extrinsic mechanisms that can also activate the forbidden LO-phonon scattering. For example, Pinzcuk and Burstein[10] have shown that surface electric fields produced by depletion layers in semiconductors can

result in forbidden LO-phonon scattering. Several workers have suggested that defects can relax momentum conservation and allow phonons normally forbidden by selection rules to participate. It was suggested that this extrinsic process can be stronger than the intrinsic process for two reasons. The first is that the q-dependent Fröhlich interaction increases in strength as q^2. Thus a process that allows phonons with larger q to participate is favored. The second is that the relaxation of momentum conservation leads to a strong double-resonance effect. Gogolin and Rashba[11] have proposed an extrinsic mechanism that involves elastic scattering between free excitons and defects. This Raman process involves fourth-order perturbation theory and can be represented by the Feynman diagram shown in Fig. 1(b), except for the fact that Gogolin and Rashba assumed the intermediate states to be discrete exciton states. This assumption is not realistic for GaAs because the exciton binding energy is very small. It is more realistic to assume that uncorrelated electrons or holes are involved. Such a modification of the theory of Gogolin and Rashba has recently been proposed by Menendez and Cardona, hereafter referred to as (MC).[12] The details of their theory will be presented in Sec. III.

III. MICROSCOPIC THEORY OF RAMAN SCATTERING IN A CRYSTAL WITH DEFECTS

We now consider how the presence of defects will modify the above description. In this section we will examine three different microscopic mechanisms for Raman scattering involving defects.

First we briefly summarize the effect of defects on the vibrational modes observed in a solid. The introduction of point defects can influence Raman scattering by allowing three new categories of vibrational modes to appear in the Raman spectrum.

(i) Localized modes. These types of vibrations occur when atoms in the immediate vicinity of a defect vibrate at frequencies different from those of the phonons found in the perfect crystal.

(ii) Resonance modes. These modes result when the frequency of the defect vibration lies within the phonon bands of the perfect crystal. The amplitudes of the resonance modes are enhanced near the defect but closely resemble the bulk phonon modes at distances far away from the defect. In general the frequency spread of such modes is broader than that exhibited by local modes and depends on the density of bulk phonons at the defect vibrational frequency.

(iii) Defect-Activated first-order Raman modes. If bulk electrons or phonons are scattered by defects, then they will no longer have a well-defined wave vector and hence momentum conservation is relaxed in the Raman process. As a result it becomes possible for phonons from throughout the Brillouin zone to participate in one-phonon Raman scattering. This type of Raman scattering has been labeled as disorder-activated first-order Raman scattering (DAFORS). The disorder responsible for previous observations of DAFORS has been introduced in a variety of ways including the creation of microcrystallites of finite size,[13] ion implantation,[14] and alloying.[15] The line shape of the DAFORS has been found to roughly reproduce the phonon density of states. There are three models which have been proposed to explain DAFORS.

A. Spatially confined phonon model (or spatial correlation model).

Several variations of this mechanism have appeared in the literature and have been given different names. It was first proposed by Shuker and Gammon[16] to explain the Raman spectra in amorphous silicon. They assumed that the electronic system is undisturbed by disorder; only the phonon system is affected. It is also assumed that the only difference between Raman scattering in a disordered solid and in a perfect crystal is that in the former case the phonon is confined spatially and therefore does not have a well-defined quasimomentum.

To make this model quantitative one can assume that the wave function of the confined phonon $\Psi_L(\mathbf{q}_0,\mathbf{r})$ has the form

$$\Psi_L(\mathbf{q}_0,\mathbf{r})=\exp(-2r^2/L^2)\phi(\mathbf{q}_0,\mathbf{r}) , \tag{6}$$

where

$$\phi(\mathbf{q}_0,\mathbf{r})=u(\mathbf{q}_0)\exp(-i\mathbf{q}_0\cdot\mathbf{r}) \tag{7}$$

is the corresponding phonon in the perfect crystal with wave vector $\mathbf{q}_0$, and L characterizes the spatial extent of the confined phonon. Upon Fourier transformation the confined phonon is found to have a distribution of wave vectors. The distribution function is given by

$$C(\mathbf{q}_0,\mathbf{q}')=(2\pi)^{-3}\int d^3r\psi'_L(\mathbf{q}_0,\mathbf{r})\exp(-i\mathbf{q}'\cdot\mathbf{r})$$
$$=L(2\pi)^{-3/2}\exp\left[\frac{-L^2|\mathbf{q}_0-\mathbf{q}'|^2}{4}\right] . \tag{8}$$

Substituting the phonon wave function in Eq. (6) into Eq. (1) gives the cross section for first-order scattering by a confined phonon of frequency ω_p and wave vector $\mathbf{q}_0$ as

$$\sigma(\omega_p)\propto D(\omega_p)\left|\omega_p^{-1/2}\int\frac{d^3k_a C(\mathbf{q}_0,0)}{(\hbar\omega_a-\hbar\omega_i)(\hbar\omega_b-\hbar\omega_s)}\right|^2$$
$$\propto\frac{D(\omega_p)}{\omega_p}\left|C(\mathbf{q}_0,0)\right|^2 . \tag{9}$$

Equation (9) gives the line shape of DAFORS that occurs via this spatial correlation (SC) mechanism. Note that if $|C|^2$ does not change appreciably as $\mathbf{q}_0$ varies within the Brillouin zone, as would be the case if $L\leq a_0$, then the line shape approximately reproduces the phonon density of states $D(\omega_p)$.

Even though momentum conservation is now not required in the electron-phonon scattering, the possible values of the intermediate electron-state momenta $\mathbf{k}_1$ and $\mathbf{k}_2$ are still subject to the constraint $\mathbf{k}_1=\mathbf{k}_2$ because of momentum conservation during the photon absorption and emission processes, i.e.,

$$\mathbf{k}_i=\mathbf{k}_1-\mathbf{k}_3\simeq 0$$

in absorption and

$$\mathbf{k}_s = \mathbf{k}_2 - \mathbf{k}_3 \simeq 0$$

in emission implies that

$$\mathbf{k}_1 \simeq \mathbf{k}_2 .$$

Thus the electronic intermediate states involved in these Raman processes are the same as for the case of the allowed TO-phonon scattering in a perfect crystal. It follows that, except for the differences in the electron-phonon interaction matrix elements, the expression for $\sigma(\omega_i)$ in this model is identical to that of the TO phonon in a perfect crystal given in Eq. (4). This is because as long as the electronic states responsible for the enhancement are assumed to be the same in the two cases, perturbation theory will produce the same frequency dependence in $\sigma(\omega_i)$.

In a perfect crystal we have pointed out that the q-dependent-electron—LO-phonon Fröhlich interaction can sharpen the RRS line shape. Similarly, in a polar semiconductor like GaAs, acoustic phonons with small q can produce macroscopic electric fields via the q-dependent piezoelectric effect. From Eq. (6) we note that spatially confined zone-edge acoustic phonons can possess small q Fourier components and can therefore possess a stronger resonance just like the forbidden LO phonon.

B. Kawamura-Tsu-Esaki model

The SC model assumes that the disorder that activates the forbidden Raman scattering affects only the vibrational modes. It is also possible that disorder alters the electronic states of the scattering medium and hence causes new Raman processes to become allowed. A theory of DAFORS due to electronic disorder was proposed by Kawamura, Tsu, and Esaki (KTE).[17] They assume that the electronic wave functions are no longer plane waves characterized by a single wave vector but instead involve a Fourier sum over a range of wave vectors:

$$\Phi_{\mathbf{k}}^{L}(\mathbf{R}) = \int d^3k' g_{\mathbf{k}}(\mathbf{k}-\mathbf{k}') \exp(i\mathbf{k}'\cdot\mathbf{R}) . \tag{10}$$

In Eq. (10) the subscript $\mathbf{k}$ denotes the wave vector of the unperturbed wave function. The function $g(\mathbf{k}')$ is the Fourier transform of the perturbed electronic wave function $\Phi_{\mathbf{k}}^{L}$ and is thus analogous to the function $C(\mathbf{q})$ that appears in the SC model.

As a result of Eq. (10), electronic transitions do not have to conserve wave vector. This allows additional electronic states to participate in Raman scattering that would otherwise be forbidden by momentum conservation. Since all three vertices in the Feynman diagram involve electronic transitions, this type of disorder-activated Raman scattering can involve one, two, or three momentum nonconserving steps. However, if the amount of disorder is not too great, then processes with only one momentum nonconserving step should be most significant. For such processes, as in the SC model, momentum conservation at the other two vertices constrains the electronic states to be the same as in the case of allowed Raman scattering. An example of a scattering process involving localized electronic states is shown in Fig. 1(c). The corresponding Raman cross section obtained by KTE, assuming that only the electron-phonon scattering does not conserve momentum, is given by

$$\sigma(\omega_p) \propto \sum_{\mathbf{q}} \left| \omega_p^{-1/2} \int \frac{d^3k_a \left[\int d^3k' g_{\mathbf{k}_a}(\mathbf{k}'+\mathbf{q}) g_{\mathbf{k}_a}(\mathbf{k}') \right]}{(\hbar\omega_a - \hbar\omega_i)(\hbar\omega_b - \hbar\omega_s)} \right|^2 , \tag{11}$$

where $\mathbf{k}_a$ and $\mathbf{k}_b$ are the wave vectors of the electron (hole) in the first intermediate states $|\mathrm{a}\rangle$ and $|\mathrm{b}\rangle$, respectively. Since momentum is still assumed to be conserved in the electron-photon interactions, $\mathbf{k}_a \simeq \mathbf{k}_i \simeq \mathbf{k}_s \simeq \mathbf{k}_b \simeq 0$. If the function $g_{\mathbf{k}}$ does not depend on $\mathbf{k}$, (i.e., all of the electronic wave functions within the band are perturbed in the same way), then

$$\sigma(\omega_p) \propto \frac{D(\omega_p)}{\omega_p} |C'(\mathbf{q})|^2 , \tag{12}$$

where

$$C'(\mathbf{q}) \equiv \int d^3k' g^*_{\mathbf{k}'}(\mathbf{k}'+\mathbf{q}) g_{\mathbf{k}'}(\mathbf{k}') .$$

Thus, the KTE model and the SC model predict the same resonance line shape unless additional electronic resonances are introduced by defects. For example an electronic resonance due to a deep center may lead to a sharpening of the RRS line shape. This is because in general the RRS line shape will be sharper near an isolated resonance than near a critical point in a continuum.

C. Defect-Mediated higher-order processes

A third possible mechanism for defect-activated Raman scattering is represented by the Feynman diagram in Fig. 1(b). In these types of processes an electron or a hole undergoes elastic scatterings with a defect in addition to scattering with a phonon. Since momentum is transferred to the defect during the elastic scattering, phonons from throughout the Brillouin zone are allowed to participate in one-phonon Raman scattering. Thus this mechanism also predicts Raman line shapes that resemble the phonon density of states. (However, it should be noted that at resonance, double-resonance effects can distort the line shapes by favoring those phonons with "special" wave vectors that allow the double-resonance condition to be satisfied.) On the other hand, the resonance enhancement of the Raman intensity predicted by this model can be quite different from that predicted by the SC and KTE mechanisms. This difference can be an important means to distinguish this mechanism from the other two mechanisms.

The defect-mediated scattering theory proposed by MC to explain the forbidden LO-phonon scattering in impure GaAs can be readily modified to apply to scattering by defect-activated Raman modes. With this in mind, we will describe the MC theory in some detail.

In deriving their results MC draw on the result of an earlier theory for allowed two-phonon scattering due to Zeyher.[18] The Feynman diagram for this two-phonon scattering process is shown in Fig. 1(d). Comparison with Fig. 1(b) shows that formally these processes are quite

similar; Fig. 1(b) is obtained from Fig. 1(d) by replacing an electron-phonon vertex with an electron-defect vertex.

Zeyher calculated the two (optical) phonon scattering cross section by a Green function approach. The underlying assumptions are the following.

Only two-band processes are considered.

Parabolic bands are assumed.

Exciton effects are neglected.

Two types of electron-phonon couplings are considered: (i) q-dependent intraband Fröhlich coupling (for the LO phonon) and (ii) deformation-potential coupling for both the TO and LO phonons.

The phonons are assumed to be dispersionless.

Zeyher finds that the cross sections for the two TO-phonon and the two LO-phonon scattering are given, respectively, by

$$\left.\frac{d\sigma}{d\Omega}\right|_{2\mathrm{TO}} \propto \int_0^{x_{\mathrm{BZ}}} dx\, x^2 \,|\, A(s_h x,-s_h x,x_1,x_2,x_3)\,|^2 , \tag{13a}$$

$$\left.\frac{d\sigma}{d\Omega}\right|_{2\mathrm{LO}} \propto \int_0^{x_{\mathrm{BZ}}} \frac{dx}{x^2} \,|\, A(s_e x,-s_e x,x_1,x_2,x_3)+A(s_h x,-s_h x,x_1,x_2,x_3)$$

$$-A(s_e x,s_h x,x_1,x_2,x_3)-A(s_h x,s_e x,x_1,x_2,x_3)\,|^2 , \tag{13b}$$

where the symbols used in Eq. (13) are defined as follows: $\mathbf{q}\equiv$ phonon wave vector $\simeq$ wave vector of the electron-hole pair,

$$x\equiv aq,\quad x_j\equiv ak_j,\quad a\equiv\left[\frac{\hbar^2}{2\mu\hbar\omega_{\mathrm{LO}}}\right]^{1/2},$$

$$k_j\equiv\left[\frac{2\mu}{\hbar^2}[\hbar\omega_i+i\Gamma-\hbar\omega_0-(j-1)\hbar\omega_p-\delta_{j2}\hbar^2q^2/(2M)]\right]^{1/2},\quad j=1,2,3,$$

$$s_{e,h}\equiv m_{e,h}/(m_e+m_h);\quad M\equiv m_e+m_h,$$

$$A(0,\lambda_2\mathbf{q},k_1,k_2,k_3)\equiv\frac{16\pi^2}{(k_1^2-k_2^2)\lambda_2 q}\left[\tan^{-1}\left[\frac{i\lambda_2 q}{k_1+k_3}\right]-\tan^{-1}\left[\frac{i\lambda_2 q}{k_2+k_3}\right]\right],$$

$$A(\lambda_1\mathbf{q},\lambda_2\mathbf{q},k_1,k_2,k_3)\equiv\frac{\lambda_1}{\lambda_1+\lambda_2}A(0,\lambda_1\mathbf{q},S^{1/2},k_2,k_1)+\frac{\lambda_2}{\lambda_1+\lambda_2}A(0,\lambda_2\mathbf{q},S^{1/2},k_2,k_3),$$

$$S\equiv\frac{\lambda_1k_3^2+\lambda_2k_1^2}{\lambda_1+\lambda_2}-\lambda_1\lambda_2q^2 .$$

MC use Zeyher's result to obtain the Raman cross section of the forbidden LO phonon by simply replacing one of the electron-phonon interaction vertices with an elastic electron- or hole-scattering vertex. They assume a q-dependent electron- (or hole-) defect scattering potential $V(q)$ of the form

$$V(q)\propto(q^2+q_F^2)^{-1}, \tag{14}$$

where $q_F\sim 2/\lambda$ and λ is the mean distance between defects. The qualitative features of their results are not very sensitive to the details of the potential chosen and are particularly insensitive to the exact choice of q_F. In addition they neglect multiple scatterings of electrons by defects and apply the Born approximation in obtaining the cross section for the LO phonon calculated from Fig. 1(b):

$$\sigma_{\mathrm{LO}}(\omega_i)\propto\int_0^{q_{\mathrm{BZ}}}\left[\frac{dq\,|\,A_T(\omega_i)\,|^2}{(q^2+q_F^2)^2}\right], \tag{15a}$$

where q_{BZ} is the wave vector at the zone boundary and

$$A_T(\omega_i)=A(s_e x,-s_e x,x_1,x_2,x_3)+A(s_h x,-s_h x,x_1,x_2,x_3)-A(s_e x,s_h x,x_1,x_2,x_3)$$
$$-A(s_h x,s_e x,x_1,x_2,x_3)+A(s_e x,-s_e x,x_1,x_2',x_3)+A(s_h x,-s_h x,x_1,x_2',x_3)$$
$$-A(s_e x,s_h x,x_1,x_2',x_3)-A(s_h x,s_e x,x_1,x_2',x_3) . \tag{15b}$$

The notation in Eq. (15b) is the same as in Eq. (13) except now

$$x_2' = ak_2' \ ;$$

$$k_3 = \left[\frac{2\mu}{\hbar^2}\right]^{1/2} (\hbar\omega_i + i\Gamma - \hbar\omega_0 - \hbar\omega_p)^{1/2}, \quad \mathrm{Im}k_3 > 0 \ ,$$

$$k_2' = \left[\frac{2\mu}{\hbar^2}\right]^{1/2} \left\{\hbar\omega_i + i\Gamma - \hbar\omega_0 - \frac{\hbar^2(x/a)^2}{2(m_e+m_n)}\right]^{1/2}, \quad \mathrm{Im}k_2' > 0 \ .$$

Plots of the RRS line shape predicted by Eq. (15) for various values of q are shown in Fig. 4(b). A discussion of these plots will be presented later in Sec. VI B when they are compared with experimental results.

The theory of MC can be readily modified to apply to DAFORS providing the following points are kept in mind.

(i) If the DAFORS involves acoustic phonons, then the dispersion of the phonon branch must be taken into account.

(ii) If the DAFORS involves zone-edge acoustic phonons, then q-dependent electron-phonon interactions such as the piezoelectric or Fröhlich interactions are not significant. We assume that the electron-phonon interaction is q independent.

(iii) For scattering involving zone-center optical phonons such as that treated by Zeyher and by MC, symmetry considerations place certain constraints on the electron-phonon scattering. Specifically, if the phonons have Γ_{15} symmetry, the electron-phonon matrix element for deformation-potential scattering is zero for electrons in the nondegenerate Γ_1 conduction band. On the other hand the hole-phonon matrix element for deformation-potential scattering is nonzero. For DAFORS involving non-zone-center phonons this restriction no longer applies and both electron- and hole-phonon scattering have to be considered.

Since the phonons with different wave vectors from a given branch represent distinct final states, it is appropriate to square the matrix elements and then integrate over the final distribution of states. The expression for the RRS line shape is then given by

$$\sigma_j(\omega_i,\omega_s) \propto \int_0^{q_{BZ}} dq\, q^2 \,|\, A_T(q,\omega_i)\,|^2 \delta[\omega_i - \omega_s - \omega_j(q)] \ , \tag{16}$$

where $\omega_j(q)$ is the frequency of the jth phonon branch.

A fourth-order Raman process can also involve various types of non-plane-wave phonons such as local modes or resonant modes. Let us first consider the case in which a local mode is involved. Then each phonon has a broad distribution of q components which can be described by a function $C(q)$ [see Eq. (8) in the limit $L \to 0$]. The various q components of this local mode do not represent distinct final states. Therefore it is appropriate to carry out the integration over q *before* squaring the matrix elements. The expression for the RRS line shape is then

$$\sigma(\omega_i,\omega_s) \propto \left| \int_0^{q_{BZ}} dq\, q^2 C(q) A_T(\omega_i) \delta(\omega_i - \omega_s - \omega_p) \right|^2 . \tag{17}$$

It is instructive to examine the magnitude of the contributions made by the different q components to the integrand of Eq. (17). This is plotted in Fig. 4(a) using parameters appropriate for GaAs. It is seen that the magnitude of the contribution from a small range of q values centered about $q = 0.1/a_0$, where a_0 is the lattice constant, is much greater than the contribution from any of the other

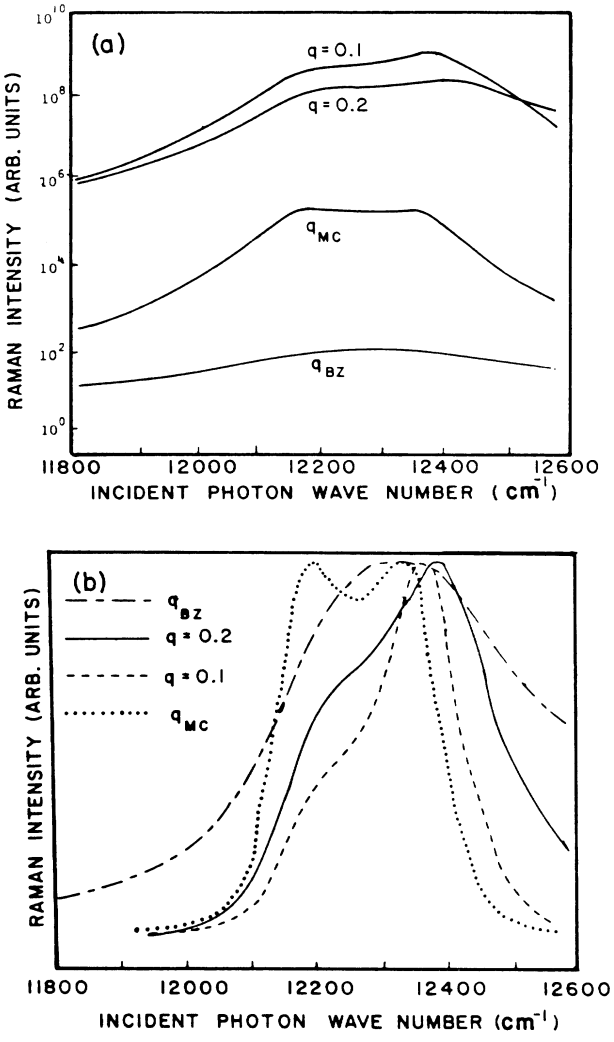

FIG. 4. Resonance behavior of the Raman cross section according to the MC theory for phonons of different q. The q values given in the figure are in units of $1/a_0$, where a_0 is the lattice constant. $q_{MC} = 0.02$ corresponds to the wave vector determined by momentum conservation for the experimental conditions described in Sec. IV. q_{BZ} is the zone-edge wave vector. (a) Here the curves are not normalized so the magnitude of the contribution from different q components can be compared. Note the log scale. (b) Here the curves are scaled to have the same peak amplitudes. This facilitates comparison of their line shapes.

q components (note log scale). These special q values correspond to scattering wave vectors that allow the double-resonance condition to be satisfied. Since a small region in q space contributes dominantly to the cross section, interference effects should not be important and the theoretical results are relatively insensitive to whether one sums and then squares the different q components as in Eq. (17) or squares and then sums as in Eq. (16). In Fig. 4(b) the line shapes of the different q components are compared by normalizing their peak amplitudes. Note that the curves for the special q values of 0.1 and 0.2 are markedly asymmetric. They peak at the outgoing resonance and decrease rapidly away from the critical point. The curves for the other q values are broader and are symmetric about the peak, which is located midway between the ingoing and the outgoing resonance frequencies.

Non-plane-wave phonons other than local modes may also participate in a Raman process of the type illustrated in Fig. 1(b). Spatially confined phonons or resonant phonons correspond to a case that is intermediate between the case of plane-wave phonons, which leads to Eq. (16), and the case of a strictly local mode, which leads to Eq. (17). For example, consider the case of a spatially confined phonon derived from a zone-edge bulk mode. Though each distinct mode is composed of a distribution of q components, there still may be a large number of distinct modes in a narrow energy range. However, as discussed above, there is no significant differece between the line shapes given by Eqs. (16) and (17) so it is not important to know *a priori* the nature of the phonon in order to predict the enhancement of its Raman cross section.

IV. EXPERIMENTAL ASPECTS

The starting material for these experiments was semi-insulating liquid-encapsulated Czochralski- (LEC) grown GaAs. One sample was uniformly irradiated with a flux of 3×10^{17} cm^{-2} fast (50-keV) neutrons produced by the FRJ-1 reactor of the Kernforschungsanlage at Jülich under conditions similar to those described by Worner *et al.*[19] The (110) surface of a second sample was irradiated with a flux of 1.0×10^{16} cm^{-2} 1.6-MeV electrons produced by a Van de Graaf generator. The beam was focused to a diameter of approximately 3 mm as estimated from viewing a fluorescent screen placed in the beam at the sample position. Assuming a Gaussian beam profile, we estimate that the peak intensity of the beam is approximately 1.1×10^{17} cm^{-2}. Since the beam size is smaller than the sample dimensions, the sample is inhomogeneously damaged. The Raman spectra for the electron-irradiated sample were recorded with the laser beam focused to a 75-μm spot at the point on the sample where the damage is at a maximum. Thus within the volume probed by the laser beam the damage is effectively homogeneous. From the estimated electron flux at this point and the fact that the defect introduction rate within the first few millimeters of the sample for irradiation with 1.6 MeV electrons is[20]

$$1 \text{ incident electron/cm}^2 \leftrightarrow 6 \text{ total defects/cm}^3 ,$$

we estimate that the *total* defect density in the region under investigation is 5×10^{17} cm^{-3}.

The Raman spectra were recorded in a near backscattering geometry from either (110) or (111) surfaces. The sample was placed in an optical dewar and cooled to temperatures between 10 and 100 K. Approximately 200 mW of excitation light was provided by a Styryl 9 dye laser pumped by an Ar^+ laser. The dye laser was tunable from 1.45 to 1.55 eV, which encompasses the fundamental band gap of GaAs. The scattered light was dispersed by a 3/4-m double spectrometer and detected as single photons by a cooled photomultiplier tube with a GaAs photocathode. Since the sensitivity of the tube falls off sharply below 1.47 eV, the spectra were corrected for the spectral response of the system. The Raman spectra were also corrected for the frequency dependence of the absorption and reflectivity of the samples.

V. EXPERIMENTAL RESULTS

In Fig. 5 we show the Stokes Raman spectra recorded from (110) surfaces for an electron-irradiated sample. Spectra recorded in the neutron-irradiated sample are qualitatively similar to the spectra shown in Fig. 5 in the frequency region below the TO phonon. The spectra of the irradiated samples differ significantly from that of the unirradiated sample; the irradiated samples show three new Raman peaks that we have labeled *A*, *B*, and *C*.

As mentioned above, the electron-irradiated sample was inhomogeneously damaged because the cross section of the electron beam was smaller than that of the sample. When the exciting laser beam is focused on an arbitrary point on this sample, the Raman spectra below the TO-phonon frequency can typically be interpreted as a super-

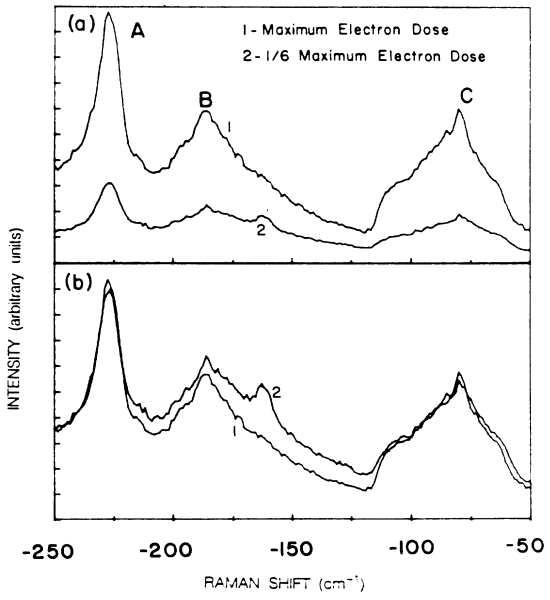

FIG. 5. Comparison of the Raman line shape of electron-irradiated GaAs for two different electron dosages. In (a) the spectra are shown with their absolute intensities while in (b) their intensities have been normalized at peak *C*.

position of two types of scattering: (i) allowed two-phonon overtone scattering and (ii) disorder-related scattering. For example, the curve labeled 2 in Fig. 5 has, in addition to the disorder-related peaks, a peak at 160 cm^{-1} which we identify has allowed overtone scattering involving two TA phonons. By monitoring the relative contribution of these two components as a function of laser-beam position on the sample, it is possible to map out a "damage profile." The diameter of the damaged region determined in this manner is 3 mm, in good agreement with the electron-beam profile. In the central 0.5 mm of the irradiated region, the damage is large enough for the disorder-induced scattering to overwhelm the two-phonon scattering (see the curve labeled 1 in Fig. 5), so this region was chosen for further study.

To help identify the defects responsible for the observed spectra, we subjected several pieces of the neutron-irradiated sample to isochronal (one-hour) annealing at temperatures ranging from 220 to 600 °C. The results are shown in Fig. 6. The relative intensities of these spectra have been normalized by the TO-phonon intensity. Peaks *A*, *B*, and *C* remain unchanged in the sample annealed to 220 °C but decrease sharply in the sample annealed to 320 °C. By 440 °C only a weak "density-of-states-like" structure is evident. The sharp peak *A* is no longer present. For the sample annealed to 600 °C (not shown) a strong band-edge luminescence was observed and it masked whatever Raman signal might be present.

In contrast with the acoustic-phonon energy region, which shows a considerably amount of disorder-related scattering, the optical phonons appear relatively unchanged by the irradiation. No change was detectable in the optical phonon spectrum of the neutron-irradiated sample even when examined with 1-cm^{-1} resolution at 10 K. In the electron-irradiated samples only the LO-phonon line shape appears to be slightly asymmetrical, having a greater intensity in the low-energy tail than in the high-energy tail.

Figure 7 shows RRS results for the allowed TO-phonon scattering in the electron-irradiated sample. It turns out that the observed variation in the intensity $I_{TO}(\omega_i)$ is dominated by the large changes in the scattering volume due to the rapidly varying penetration depth of the light near the absorption edge of GaAs. We have corrected

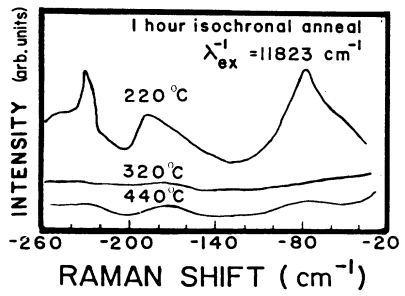

FIG. 6. Stokes Raman spectra recorded for the neutron-irradiated sample following one-hour isochronal annealing. The intensity of the spectrum for the sample annealed to 220 °C is unchanged compared to the unannealed sample.

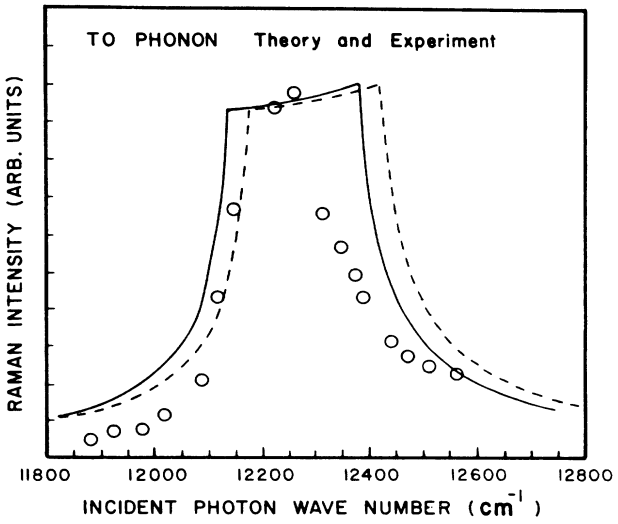

FIG. 7. Resonance behavior of allowed TO-phonon scattering at 100 K in electron-irradiated GaAs. Experimental data have been corrected for absorption and other effects listed in the text (open circles). Also shown are fits of Eq. (4) to the corrected experimental data using $\omega_0 = 12\,160$ cm^{-1} (dashed line) and $\omega_0 = 12\,120$ cm^{-1} (solid line). No damping is included.

these data using the measured absorption spectra. (See Fig. 1 of Ref. 21.) We found that the electron-irradiated sample still exhibits a clear exciton peak but that the absorption edge is shifted down in energy by 20 cm^{-1} relative to the unirradiated sample. This small shift may be due to local strains introduced by the irradiation. In the energy range at and above the absorption edge, these spectra look very similar to those reported in the literature.[22] At energies below the band gap the irradiated samples show increased absorption. This can be attributed to the presence of defect-induced band-tail states. The neutron-irradiated sample shows far greater defect-induced subband gap absorption than the electron-irradiated sample.[23] In addition to the absorption correction, the data in Fig. 7 have been corrected for variations in the sample reflectivity and for the ω^4 dependence of the scattering cross section.

Figures 8 and 9 show the enhancement for the LO-phonon intensity *relative* to the TO-phonon intensity for the electron- and neutron-irradiated samples, respectively. In both cases the result is a fairly sharp peak. The steepness of this peak on the low-energy side implies that the enhancement in the LO-phonon cross section must be much stronger than the TO phonon. Indicated in Figs. 8 and 9 by arrows are the locations of the peaks of the enhancement line shapes. Also shown for comparison is the location of the energy gap. For the forbidden LO phonon this peak occurs at $12\,470 \pm 30$ cm^{-1} in both Figs. 8 and 9. It should be noted that this is one full LO-phonon frequency above the gap, which was determined by absorption to be at $12\,160 \pm 40$ cm^{-1}. Thus the peak of the RRS line shape for the forbidden LO-phonon scattering occurs at the outgoing resonance.

Figures 8 and 9 also show plots of the cross sections for

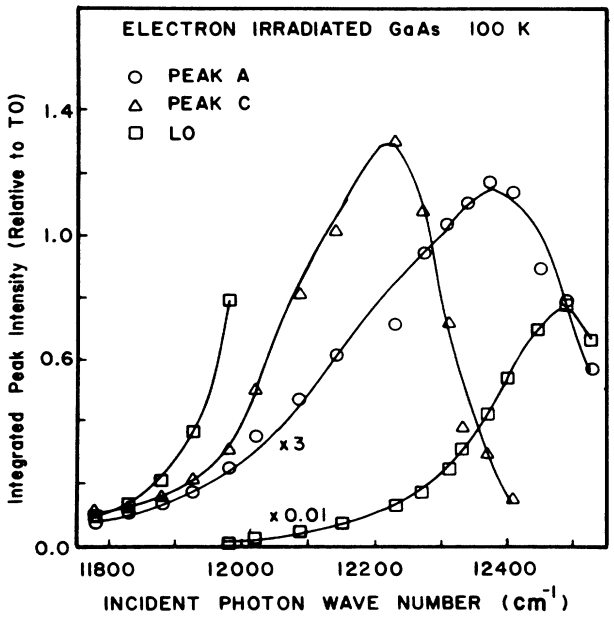

FIG. 8. RRS behavior of peak A, peak C, and the LO phonon in electron-irradiated GaAs at 100 K. These were recorded in a $\Gamma_1+4\Gamma_{12}$ scattering geometry. Solid lines are to guide the eyes only.

the defect-induced peaks A and C relative to the TO phonon for the electron- and the neutron-irradiated samples, respectively. The most noteworthy feature of these data is that, with the exception of peak C in the neutron-irradiated sample, all of these peaks exhibit enhancements that are stronger than that of the TO phonon, although not as strong as the LO phonon.

A second important result is that the maximum of the resonance enhancement for peak A occurs at the outgoing resonance in both Figs. 8 and 9. The frequency of peak C is only 80 cm^{-1} so it is not possible to determine whether the peak in the enhancement occurs at the outgoing resonance or at a point midway between the incoming and the outgoing resonances.

Figure 10(a) shows a comparison between the RRS results for peak A in the electron-irradiated GaAs recorded at 100 K and results recorded at 10 K. The corresponding results for the forbidden LO phonon are shown in Fig. 10(b). In both cases lowering the temperature causes an upward shift of 70 cm^{-1} in the location of the enhancement peak. This is roughly the amount that the band gap

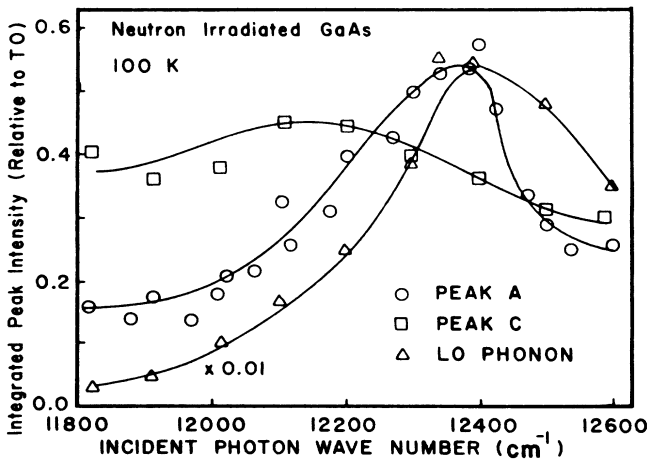

FIG. 9. RRS behavior of peak A, peak C, and LO-phonon scattering in the neutron-irradiated sample at 100 K. These were recorded in a $\Gamma_1+4\Gamma_{12}$ scattering geometry. Solid lines are to guide the eyes only.

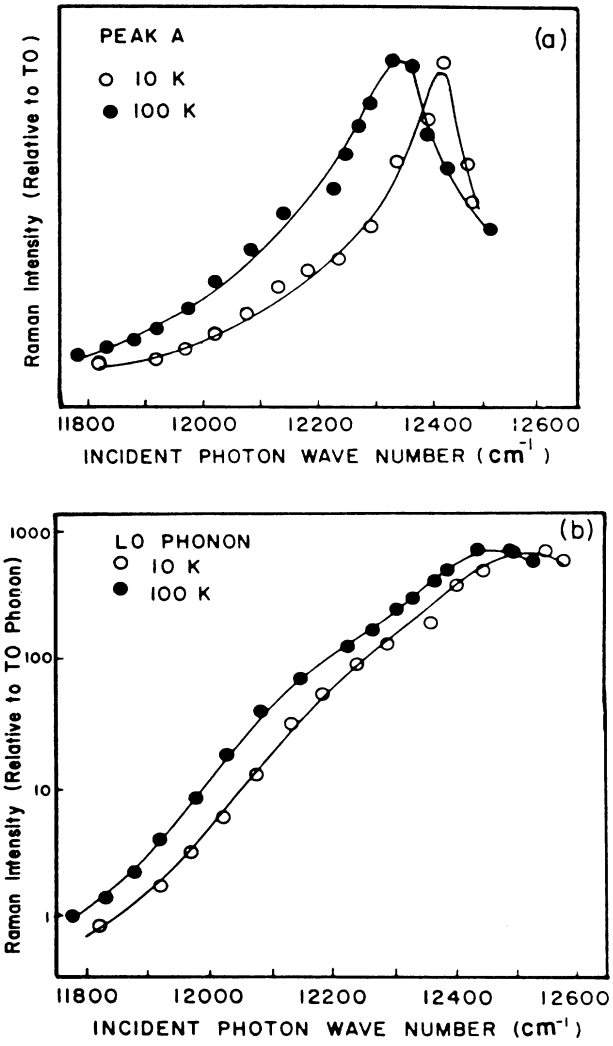

FIG. 10. Temperature dependence of RRS in the electron-irradiated sample. (a) Peak A relative to TO phonon at 10 and 100 K. (b) LO-phonon relative to TO-phonon intensity at 10 and 100 K. Note the logarithmic scale for the intensity. In both (a) and (b) the peak amplitudes have been normalized in order to facilitate comparison of the line shapes. The amplitude of both the peak A and the LO-phonon resonances (relative to the TO phonon) was roughly 20% greater at low temperature.

is expected to shift with temperature coefficient. The line shapes of the RRS results do not change much upon lowering the temperature.

VI. DISCUSSION

A. Identification of defect-induced Raman modes

Previous studies on the nature of the damage produced by neutron and electron irradiation have produced the following general picture.[24,25] In neutron-irradiated samples the material surrounding a "primary knock-on" contains clusters of defects but are otherwise basically crystalline (i.e., it is not amorphous). For sample irradiated with a flux of 3×10^{17} neutrons/cm^2 these damaged regions occupy roughly 5% of the total sample volume. It has been proposed that the primary defects in these damaged regions are interstitial-vacancy pairs that are accompanied by local strains. Few larger defect complexes are thought to be produced. For the case of electron-irradiated GaAs the damage is thought to be more homogeneous, consisting of intrinsic point defects. This is because collisions of the lighter electron with an atom transfers only enough energy to eject a single atom. Thus the point defects that are created are spatially uncorrelated with one another.

As mentioned in Sec. III, the simple theories of DAFORS predict that the Raman line shape should resemble the phonon density of states. This is in accordance with what has been observed by a number of workers[4,14,15,17,26–30] who examined either ion-implanted GaAs or various III-V alloys. Similarly, we first identify peaks B and C in the irradiated samples as due to DAFORS, although we will point out below that this identification is not entirely consistent with our RRS results. Comparison of the spectra labeled 1 in Fig. 5 with a calculation of the phonon density of states shows that the line shape of peak B is similar to the density of states of the longitudinal-acoustic (LA) phonons while peak C reproduces the density of states of the transverse acoustic (TA) branches.

In contrast, peak A has not been observed in previous Raman studies of disordered GaAs. This peak is much different from peaks B and C in that it is much narrower (full width at half maximum is 7 cm^{-1}) and is not reproduced in the phonon density of states.[31] One may argue that peak A can be explained by the broad structure near 227 cm^{-1} in the theoretical phonon density of states that arises from the LA(X) critical point. However, this explanation is not likely based on the following observations. Firstly, the structure at 227 cm^{-1} is broader than peak A while all of the other peaks in the theoretical spectra are sharper than the corresponding peaks in the experimental spectra. Secondly, the structure near 227 cm^{-1} is weaker than the other structures in the phonon density of states while peak A is much stronger than the other DAFORS peaks. One may question the accuracy of the calculated density of states. However, other experimental evidence also shows that peak A is not a DAFORS peak. The Raman spectrum in Fig. 11 was recorded with the laser beam focused at a point 1.5 mm away from the point of maximum damage. In this figure both the disorder-induced scattering and the two-phonon overtone scattering are visible. It is well known that the two-phonon overtone spectrum roughly mirrors the phonon density of states scaled by a factor of 2.[27] Indeed, two phonon peaks corresponding to overtone scattering of peaks B and C are present (labeled $2B$ and $2C$). However, the two-phonon overtone scattering observed in the range corresponding to twice the energy of peak A [455 cm^{-1}, labeled 2LA(X)] is too broad and weak to be identified as overtone scattering of peak A; instead it is more consistent with an overtone scattering associated with the critical point LA(X) in the phonon density of states.

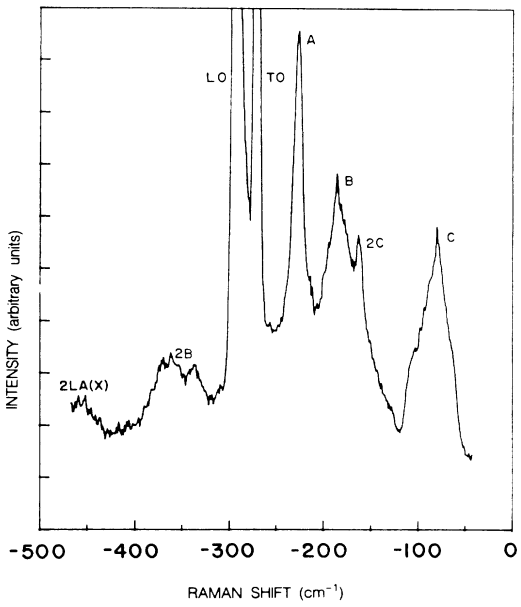

FIG. 11. Raman spectra in electron-irradiated GaAs recorded at a point where the electron dosage is lower than the maximum dosage by roughly a factor of 6.

We also rule out the possibility that peak A is due to a two-phonon-difference combination process involving emission of an optical phonon and absorption of an acoustical phonon because peak A is as strong at 10 K as at 100 K and because the corresponding two-phonon-sum combination peak is not observed. The absence of peak A in GaAs that has been disordered by a variety of other means such as ion implantation,[14,26] alloying,[17,15,27–30] or Cr doping[1] implies that it is associated with the presence of a specific defect introduced in relatively large concentrations by both neutron and electron irradiation.

We therefore identify peak A as due to either electronic or vibrational Raman scattering associated with some intrinsic defects induced by the irradiation. Electronic Raman scattering can be ruled out based on the observed resonant enhancement (Figs. 8 and 9), which is too strong to be explained by electronic Raman scattering.[32]

The Raman spectrum observed in the sample that has been annealed to 440 °C in Fig. 6 shows a weak DAFORS structure that is presumably caused by disorder that has not been annealed out. Noticeably absent from this spectrum is any evidence of the sharp peak A structure. This

suggests that peak A is associated with a defect that has a characteristic annealing temperature between 220 and 320 °C.

The sharpness of peak A suggests that it is probably associated with an isolated point defect since Raman peaks associated with large defect clusters are more likely to have considerable inhomogeneous broadening. In principle, ion implantation, like neutron and electron irradiation, will introduce also large quantities of intrinsic defects, yet peak A has not been observed in ion-implanted samples. However, as mentioned above, of the three kinds of high-energy particles (ions, neutrons, and electrons), ions, and to a lesser extent neutrons, tend to produce defect clusters while electrons produce isolated point defects. This is consistent with our observation that in the electron-irradiated sample, peak A is considerably stronger relative to the DAFORS and there is also less featureless background scattering than in the neutron-irradiated sample. The very narrow linewidth observed for peak A suggests that this peak is due to vibrational modes that are well localized around a defect.

If peak A corresponds to a vibrational mode of an intrinsic point defect, then the possible point defects are I_{Ga}, I_{As}, V_{Ga}, V_{As}, As_{Ga}, and Ga_{As}. The observed annealing behavior allows some of these to be ruled out. For example, ESR measurements in the neutron-irradiated sample show that it contains 7×10^{17} cm^3 As_{Ga} antisite defects.[33] Measurements by Worner *et al.*[19] have shown that after one-hour isochronal annealing the concentration of As_{Ga} as determined by ESR remains constant to 400 °C, above which the concentration drops sharply by a factor of 100. Thus neither the annealing dependence of peak A nor the annealing dependence of most of the DAFORS is consistent with As_{Ga} defects. However, it is possible that the weak structure remaining in the spectra of the sample which has been annealed to 400 °C is due to As_{Ga}.

An annealing stage in the vicinity of 225 °C has been reported by nearly every author who has performed an annealing experiment on either electron- or neutron-irradiated GaAs.[34] In particular, Pons and Bourgoin[35] used DLTS to observe this stage in electron-irradiated GaAs. They demonstrate that this stage is due to annealing of the so-called $E2$ electron trap. The microscopic identity of this level is not definitely known, but they present strong evidence that it is a simple defect formed by displacement of the As sublattice (i.e., V_{As}, As_{Ga}, or I_{As}). Their argument is based on an observed anisotropy in the defect introduction rate when the electron beam is incident in the [111] or $[\bar{1}\,\bar{1}\,\bar{1}]$ directions. Based on positron lifetime measurements, Cheng *et al.*[36] argue that the arsenic vacancy is the more likely possibility. Pons *et al.*[37] also conclude that the vacancy is the more likely candidate. Recently Loualiche *et al.*[38] have shown additional evidence that this annealing stage is associated with As vacancies. On this basis we tentatively conclude that peak A is most likely associated with V_{As}. The observed Γ_1 symmetry suggests a breathing vibrational mode but care should be exercised in making such an identification as it is well known that Raman selection rules often break down near resonance.[8]

Examination of the annealing results yields additional clues concerning the nature of peaks B and C. Comparison of the line shapes of the sample annealed to 320 °C with the unannealed sample reveals that not only has the overall scattering intensity diminished in the annealed sample but the line shape has lost the sharp structures that correspond to critical points in the phonon density of states and has taken on a more "washed out" appearance. This behavior can be qualitatively understood within the SC mechanism of DAFORS discussed above. The SC mechanism predicts that as the localization length L becomes longer, scattering involving zone-edge phonons will become weaker. Thus the "washed out" line shape observed in the annealed sample simply results from the decrease in defect concentration.

On the other hand, this explanation cannot account for the reappearance of the sharp density-of-states-like Raman structure in the sample annealed to 440 °C. Similarly, it cannot explain the Raman spectra of the samples that have been irradiated with lower electron dosages (curve 2 in Fig. 5). We will concentrate on the DAFORS peak C measured at two different locations within the electron-irradiated region of the sample. One measurement takes place at the center of the damaged region while the other was recorded at a point 1.5 mm from the center. From the measured intensities of peak C relative to the TO-phonon intensity [Fig. 5(a)], we estimate that the defect concentration differs by a factor of 6 between these two points. (This estimate is roughly consistent with the measured beam size of 3 mm in diameter assuming a Gaussian profile.) In spite of the significant difference in defect concentration, the *shape* of the DAFORS peaks observed at these two locations is identical [Fig. 5(b)].

The phonons responsible for peak C could be spatially confined phonons, resonant phonons, or plane-wave phonons. Spatially confined phonons are expected to have localization lengths that depend on the separation between defects while the spatial extent of resonance modes, which are associated with isolated defects, should be independent of the defect concentration. Obviously, the spatial extent of a plane-wave phonon also does not depend on the defect concentration. The insensitivity of the peak-C line shape to electron dosage suggests that in the electron-irradiated samples this peak is due mostly to scattering involving either resonant phonons or plane-wave phonons. On the other hand, the same peak C in the neutron-irradiated sample seems to be mostly due to confined phonon modes. We will present additional evidence to support this hypothesis based on the RRS results.

A number of previous studies have focused on the broadening, asymmetry, and red-shift of the LO-phonon peaks induced by defects.[13–15] These effects have been successfully explained by the SC model. We have been unable to detect any distortion of the LO-phonon line shape in the neutron-irradiated sample and only a small asymmetry and broadening in the electron-irradiated sample. Our explanation is that although the amount of defects in the neutron-irradiated sample is larger, these defects form clusters which produce very broadened optical-phonon peaks. The observed sharp LO peaks in the neutron-irradiated sample originate from the 95% of

the sample volume that is relatively undamaged while the weak DAFORS from the damaged remaining 5% of the sample is completely negligible. On the other hand, the defects in the electron-irradiated sample are more homogeneously distributed and cause a slight distortion of the phonon line shapes.

B. Resonance behavior

We now compare the experimentally observed resonance behaviors with the predictions of the theories presented in Sec. II.

1. TO phonon

Figure 7 shows a fit of Eq. (4) to the corrected TO-phonon cross section in the electron-irradiated sample. There are three adjustable parameters used in obtaining this fit: (1) peak height (since the absolute value of the measured Raman cross section is not known), (2) damping of the electron intermediate state, and (3) the band-gap energy. The theoretical line shape is quite insensitive to the damping parameter provided that the damping parameter is small relative to the phonon energy. It is found that the best fit to the data is achieved in the limit of zero damping. Even in this limit, however, the experimental peak is 40% narrower than the theoretical line shape. This may be explained by the fact that the theory neglects exciton effects, which tend to sharpen resonances. Previous workers have also found that exciton effects improve the fit to the experimental data. However, existing theories such as those of Trommer and Cardona,[7] Shah, Leite, and Damen,[39] and Ferrari and Luzzi[40] that take exciton effects into account also assume that the phonon frequency is zero so they are not accurate in the immediate vicinity of the enhancement peak. The fit also gives a band-gap frequency of $12\,120\pm40$ cm^{-1}, whereas a value of $12\,170\pm20$ cm^{-1} is deduced from the absorption measurements. Again this small discrepancy can be qualitatively accounted for by exciton effects which will shift the resonance peak downward by about 34 cm^{-1} in GaAs. Also, models that include exciton effects predict asymmetric line shapes in which the low-energy side rises more sharply than the high-energy side. Such asymmetry is evident in the experimental result in Fig. 7.

Thus we conclude that the standard model without damping and exciton effects gives a reasonably good description of the observed TO-phonon resonance line shape. Since exciton effects appear to improve the quality of the fit, this implies that the damage produced by the electron irradiation in our sample is not too severe. This is consistent with the absorption spectrum, which is only slightly different from the absorption spectrum observed in the unirradiated sample. We note incidentally that this is the first detailed study of RRS at the E_0 gap of GaAs. Previous work[7] has been limited to higher-energy gaps because of the strong luminescence near the E_0 gap of GaAs.

2. LO phonon

The absorption spectrum and RRS of the TO phonon have suggested that our GaAs sample is only moderately perturbed by the electron irradiation. It is thus reasonable to apply the MC theory, which assumes elastic scattering of Bloch electrons from point defects, to interpret our LO-phonon RRS results. (Obviously, when the defect density is high enough, this model will break down as the band structure becomes severely perturbed.)

A good fit of Eq. (17) to the experimental data for the LO-phonon scattering has been previously demonstrated [see Fig. 4(c) of Ref. 21]. The value of the gap deduced from this fit was 12 160 cm^{-1}, which is in good agreement with that deduced from the TO-phonon RRS data and from the absorption measurements. The value for the damping (90 cm^{-1}) seems reasonable since it is comparable to the value deduced by MC from their results at the $E_0+\Delta_0$ gap of GaAs. Overall the theory satisfactorily explains the observed line shape, including the location of the peak at the outgoing resonance.

3. Modes A and C

In Sec. III we discussed four different Raman processes involving defects that could potentially account for the Raman peaks A and C. We will now compare theoretical line shapes with the experimental results. Such a comparison is based on the assumption, which was justified above, that the band structure in the electron-irradiated sample is not strongly perturbed by the radiation damage. If this is not the case, then there will be too many adjustable parameters and the significance of any agreement between theory and experiment is greatly diminished.

With this assumption both the KTE model and the SC mechanism with a deformation-potential type of electron-phonon interaction predict that the RRS line shapes for the defect-induced modes should be identical to that of the TO phonon. It is clear from Figs. 8 and 9 that the KTE model cannot account for the experimental results, perhaps with the exception of peak C in the neutron-irradiated sample.

It was pointed out in Sec. III A that a $\mathbf{q}$-dependent piezoelectric electron-phonon interaction could be appreciable for non-plane-wave phonons. In this case the SC mechanism becomes formally similar to the forbidden LO scattering in a perfect crystal. This theory thus predicts resonances of peaks A and C in the electron-irradiated sample that are stronger than the TO-phonon resonance. However, as in the case of the forbidden LO-phonon scattering, it is necessary that the scattering process be higher than third order in order to explain the stronger outgoing resonance observed experimentally.

However, we find that a fourth-order process involving plane-wave phonons (see Sec. III C) cannot explain the experimental resonances of peaks A and C. If peaks A and C are identified as plane-wave phonons, their frequencies suggest that they are zone-edge acoustic phonons. Then the theoretical enhancement (the curve labeled q_{BZ} in Fig. 4) turns out to be even less pronounced than the allowed TO-phonon resonance and disagrees completely with experiment. On the other hand, if the phonons responsible for A and C are not plane waves, we obtain good fits to the data of Fig. 8 [see Figs. 4(b) and 4(c) in Ref. 21]. In obtaining the theoretical curves we assumed that both

phonons are completely localized in the sense that the function $C(q)$ is a constant throughout the Brillouin zone. Otherwise there are no adjustable parameters. The values used for the gap ω_0 and the damping are the same as those used in fitting the forbidden LO-phonon scattering in Fig. 4(c) of Ref. 21. The theory accounts qualitatively for the two important features of the observed enhancement in the defect-related modes; namely, that the resonance is stronger than that of the TO phonon and peaked at the outgoing resonance. We also note that the observed resonances in peaks A and C are not as strong as for the forbidden LO phonon. The theoretical curves are able to reproduce this behavior because we have assumed that the interaction between the electrons and the defect-related phonons is q independent while the Fröhlich interaction response for the forbidden LO-phonon scattering is q dependent.

The fact that a higher-order process better describes the enhancements of peaks A and C suggests that double-resonance effects are important for the defect-induced peaks. A requirement for double resonance to be possible in our model is that non-plane-wave phonons must be involved. The reason is that double resonance is satisfied only for those phonons having specific q values defined by the band dispersions. As a result this model predicts that the RRS line shape is sensitive to the degree of localization of the phonon. This can be demonstrated by assuming that the phonon has a Gaussian envelope as was done in Sec. III A and applying Eq. (17) to calculate the RRS line shape. The results are shown in Fig. 12 for localization lengths of 5 and 100 Å. Even though 100 Å corresponds to a reasonably well-localized phonon, the RRS line shape is already quite broad (in fact, it is broader than the allowed TO-phonon resonance) and is no longer peaked at the outgoing resonance. This results from the fact that in the model of Sec. III A, $C(q)$ is very sensitive to the localization length L when $qL \geqq 1$. Thus whether

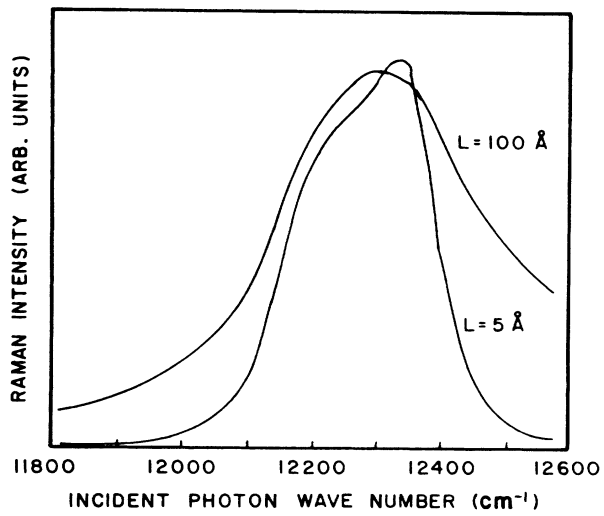

FIG. 12. Resonance behavior of a spatially confined phonon mode with calculated from Eqs. (16) and (8) for $L=5$ Å and $L=100$ Å.

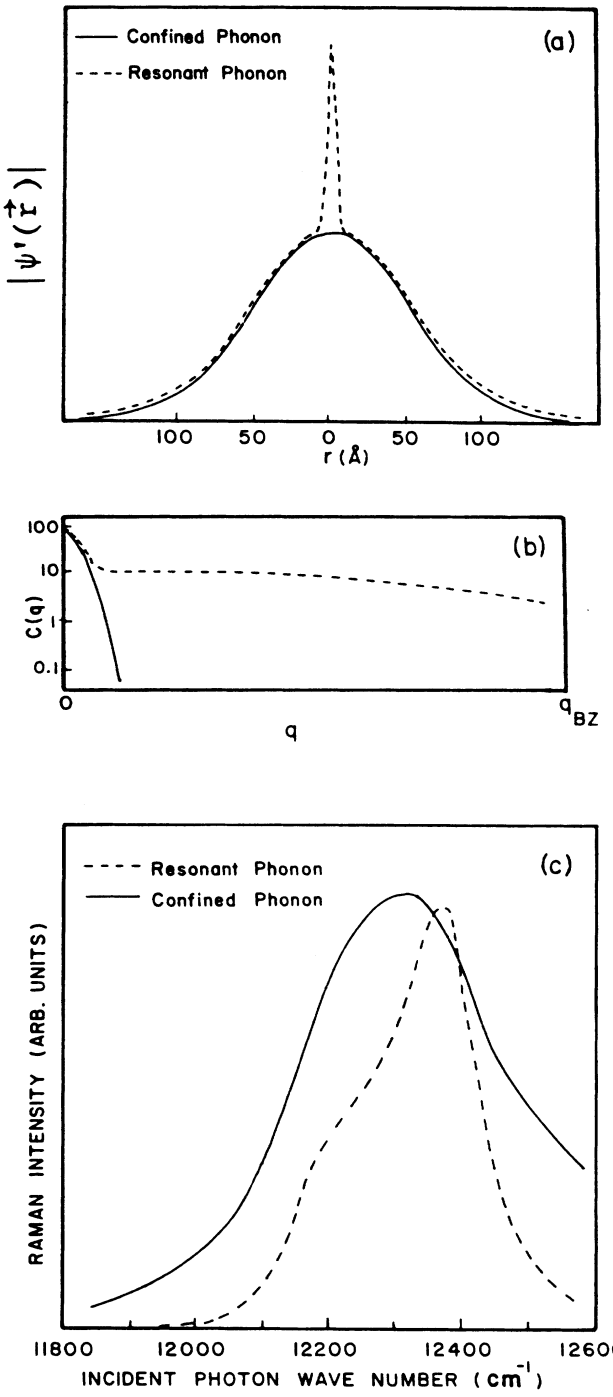

FIG. 13. Comparison between the enhancement in the Raman cross section of a resonance phonon and a spatially confined phonon. (a) Model for the wave functions of the confined and resonance phonons. The confined phonon is assumed to have an envelope given by $\exp(-2r^2/L^2)$ while the resonant phonon has an envelope given by $\exp(-2r^2/L_1^2)$ $+\exp(-2r^2/L^2)$. Here $L_1=5$ Å and $L_2=100$ Å. (b) Corresponding distribution of Fourier components for these two types of phonons. Note the logarithmic vertical scale. (c) RRS behavior for these two phonons as predicted by Eq. (16) assuming $\omega_p=80$ cm^{-1}.

double-resonance effects are important or not depends critically on L.

Our conclusion is that more localized modes give rise to sharper resonances. Examination of the experimental data for the resonance behavior of the defect-induced modes (Figs. 8 and 9) suggests that peak A is well localized in both the neutron- and the electron-irradiated samples while peak C is well localized only in the electron-irradiated sample. This is consistent with our proposal that peak C in the electron-irradiated sample involves resonance modes while peak C in the neutron-irradiated sample is probably due to either spatially confined modes or plane-wave modes and is not due to isolated defects. The difference between the electron- and neutron-irradiated samples can be traced to the fact that neutron irradiation produces defect clusters, which spatially confine the phonon modes.

Note that even though a resonant mode may extend over many lattice sites in the crystal, such modes can still have an enhanced amplitude at the defect. This enhancement will result in a broad range of Fourier components which enables a strong double resonance to occur and leads to strong resonances. As an illustration we show in Fig. 13(a) a simple model for the wave function of a resonance mode and the corresponding theoretical predictions for its RRS line shape. The wave function of this resonant mode is assumed to be a linear combination of two Gaussians [Fig. 13(a)]:

$$\Psi'(r)=\frac{1}{A}\left[\exp\left[\frac{-2r^2}{L_1^2}\right]+\exp\left[\frac{-2r^2}{L_2^2}\right]\right], \tag{18}$$

where A is the proper normalization constant. Substituting Eq. (18) into Eq. (8) gives

$$C(q)\propto L_1\exp\left[\frac{-(q')^2L_1^2}{4}\right]+L_2\exp\left[\frac{-(q')^2L_2^2}{4}\right], \tag{19}$$

where $q'\equiv q_{\mathrm{BZ}}-q$.

In Fig. 13(a), L_1 corresponds to the length over which the enhancement of the amplitude of the resonant phonon at the defect decays. L_2 is assumed to be a much longer decay length that corresponds to the spatial extent of the resonant mode. Two cases are shown in Fig. 13(a): (1) $L_1=5$ Å, $L_2=100$ Å and (2) $L_1=L_2=100$ Å. The first case corresponds to a resonant phonon in which there is an enhanced amplitude of vibration at the defect which decays rapidly away from the defect. The second case describes a confined phonon for which there is no enhanced amplitude of vibration at the defect. The corresponding functions $C(q)$ are shown in Fig. 13(b). Figure 13(c) shows the RRS line shapes predicted by the theory for the fourth-order Raman process [Eq. (17)]. The result indicates that even though these two phonons differ from one another only within the first few lattice constants surrounding the point defect, the RRS line shapes are appreciably different. *Thus the RRS line shape is sensitive to the enhanced motion in the immediate vicinity of the defect.*

VII. CONCLUSIONS

In conclusion we have been able to observe new and relatively sharp peaks due to intrinsic defects in the Raman spectra of both electron- and neutron-irradiated GaAs. The symmetry and annealing dependence of one of the peaks at 227 cm^{-1} is consistent with its identification as a vibrational mode of an As vacancy. The use of incident photons tuned to just below the band gap has allowed us to simultaneously take advantage of both the relative large scattering volume and a a large resonance enhancement. This results in large scattering intensities for the defect-related Raman processes and suggests that it should be possible to examine defect-related scattering in samples with considerably lower defect concentrations.

The enhancement of the defect-induced modes in the vicinity of the E_0 gap is explained by a theoretical model based on fourth-order perturbation theory and involves elastic scattering of the carriers by defects. Within the framework of this model it is shown that the resonant enhancement behavior is sensitive to the degree of localization of the phonon modes. The well-localized modes are found to exhibit a stronger resonant enhancement. This result further enhances the usefulness of RRS as a probe of defects. It implies that one can selectively enhance that scattering involving vibrational modes with an increased atomic motion in the immediate vicinity of the defect. It is exactly this type of mode that may contain important microscopic information concerning the defect.

Although the present work has been carried out in the vicinity of the fundamental gap, we expect double-resonance effects to also be important at higher-lying energy gaps. Resonant Raman study of defect-induced modes at higher-energy band gaps has the advantage that there will be less background luminescence from the sample to obscure the Raman signals.

ACKNOWLEDGMENTS

We are grateful to Dr. D. Goldberg of Lawrence Berkeley Laboratory for assistance in the electron irradiation of the GaAs samples and to Yi He Huang and Bo Yang Lin for technical assistance. We are indebted to Professor E. R. Weber for the neutron-irradiated GaAs sample and for many helpful discussions. The work at Berkeley was supported by the Director, Office of Energy Research, Office of Basic Energy Sciences, Materials Sciences Division of the U.S. Department of Energy under Contract No. DE-AC03-76SF00098.

[1]Some of this work has been previously published in the following papers: R. S. Berg, P. Y. Yu, and E. R. Weber, *Proceedings of the Seventeenth International Conference on the Physics of Semiconductors, San Francisco, 1984,* edited by J. Chadi and W. A. Harrison (Springer-Verlag, New York, 1985), p. 765; Appl. Phys. Lett. **47**, 515 (1985); R. S. Berg and P. Y. Yu, Phys. Rev. B **33**, 7349 (1986).

[2]F. H. Pollak and R. Tsu, Proc. Soc. Photo-Opt. Instrum. Eng.

452, 26 (1984).
[3]A. S. Barker and A. J. Sievers, Rev. Mod. Phys. **47**, S1 (1975).
[4]E. Bedel, R. Carles, A. Zwick, J. B. Renucci, and M. A. Renucci, Phys. Rev. B **30**, 5923 (1984).
[5]P. Y. Yu, M. H. Pilkuhn, and F. Evangelisti, Solid State Commun. **25**, 371 (1978).
[6]D. J. Wolford, B. G. Streetman, S. Lai, and M. V. Klein, Solid State Commun. **32**, 51 (1979).
[7]R. Trommer and M. Cardona, Phys. Rev. B **17**, 1865 (1978).
[8]*Light Scattering in Solids II,* Vol. 50 of *Topics in Applied Physics,* edited by M. Cardona and G. Güntherodt (Springer-Verlag, Berlin, 1982), p. 19.
[9]R. Martin, Phys. Rev. B **10**, 2620 (1974); **4**, 3676 (1971).
[10]A. Pinzcuk and E. Burstein, Phys. Rev. Lett. **21**, 1073 (1968).
[11]A. A. Gogolin and E. E. Rashba, Solid State Commun. **19**, 1177 (1976).
[12]J. Menendez and M. Cardona, Phys. Rev. B **31**, 3696 (1985).
[13]H. Richter, Z. P. Wang, and L. Ley, Solid State Commun. **39**, 625 (1981).
[14]K. K. Tiong, P. M. Amirtharaj, F. H. Pollak, and D. E. Aspnes, Appl. Phys. Lett. **44**, 122 (1984).
[15]P. Parayanthal and F. H. Pollak, Phys. Rev. Lett. **52**, 1822 (1984).
[16]R. Shuker and R. W. Gammon, Phys. Rev. Lett. **25**, 222 (1970).
[17]H. Kawamura, R. Tsu, and L. Esaki, Phys. Rev. Lett. **29**, 1397 (1972); R. Tsu, H. Kawamura, and L. Esaki, in *Proceedings of the Eleventh International Conference on the Physics of Semiconductors, Warsaw, 1972,* edited by M. Miasek (Elsevier, Amsterdam, 1972), p. 1135.
[18]R. Zeyher, Phys. Rev. B **9**, 4439 (1974).
[19]R. Worner, U. Kaufman, and J. Schneider, Appl. Phys. Lett. **40**, 141 (1982).
[20]K. D. Glinchuk *et al.*, Fiz. Tekh. Poluprovdn. **17**, 751 (1983) [Sov. Phys.—Semicond. **17**, 471 (1983)].
[21]R. S. Berg and P. Y. Yu, Phys. Rev. B **33**, 7349 (1986).
[22]M. D. Sturge, Phys. Rev. **127**, 768 (1962).
[23]The magnitude of the Raman signal was much larger in the electron-irradiated sample than in the neutron-irradiated sample. In addition, electron irradiation produces a more theoretically tractable result than neutron irradiation (i.e., homogeneously distributed isolated defects as opposed to inhomogeneously distributed clusters). For these reasons we shall concentrate on trying to understand quantitatively only the RRS results for the electron-irradiated sample. The RRS results for the neutron-irradiated sample will be discussed only qualitatively.
[24]K. Laithwaite and R. C. Newman, Philos. Mag. **35**, 1689 (1977).
[25]R. Coates and E. W. J. Mitchell, Adv. Phys. **24**, 593 (1975).
[26]S. Ushioda, Solid State Commun. **15**, 149 (1974).
[27]R. Carles, N. Saint-Cricq, J. B. Renucci, M. A. Renucci, and A. Zwick, Phys. Rev. B **22**, 4804 (1980).
[28]R. Carles, A. Zwick, M. A. Renucci, and J. B. Renucci, Solid State Commun. **41**, 557 (1982).
[29]N. Saint-Cricq, R. Carles, J. B. Renucci, A. Zwick, and M. A. Renucci, Solid State Commun. **39**, 1137 (1981).
[30]B. Jusserand and J. Sapriel, Phys. Rev. B **24**, 7194 (1981).
[31]G. Dolling and R. A. Crowley, Proc. Phys. Soc. London **88**, 463 (1966).
[32]P. Y. Yu, Phys. Rev. B **20**, 5286 (1979).
[33]E. R. Weber, in *Proceedings of the Conference on Semi-insulating III-V Materials, Warm Springs, 1984,* edited by D. C. Look and J. S. Blakemore (Shiva, Nantwich, England, 1984).
[34]D. V. Lang, in *Radiation Effects in Semiconductors,* edited by N. B. Urli and J. W. Corbett (Institute of Physics, London, 1976).
[35]D. Pons and J. Bourgoin, Phys. Rev. Lett. **47**, 1293 (1981).
[36]L. J. Cheng, J. P. Karins, J. W. Corbett, and L. C. Kimerling, J. Appl. Phys. **50**, 2962 (1979).
[37]D. Pons, A. Mircea, and J. Bourgoin, J. Appl. Phys. **51**, 4150 (1980).
[38]S. Loualiche, A. Nouailhat, G. Guillot, and M. Lannoo, Phys. Rev. B **30**, 5822 (1984).
[39]J. Shah, R. C. Leite, and T. C. Damen, Opt. Commun. **1**, 267 (1970).
[40]C. A. Ferrari and R. Luzzi, Phys. Rev. B **19**, 5284 (1979).